Supplementary Methods

A1. Derivation of the kinematic conflict equation

The pair (a, g) spans a continuous surgical design space, Ω, such that every point corresponds to a unique candidate operative configuration. To quantify the energetic penalty associated with kinematic conflict, we defined the total potential energy functional of the reconstructed system as follows:

$$\Pi[u] = U_{\text{int}} - W_{ext} = \iint_{\Omega} \left(\frac{1}{2} \mathbf{C} : (\nabla u \otimes \nabla u) - \tilde{f} \cdot u \right) da\,dg \tag{S1}$$

where $\mathbf{C}$ denotes the effective stiffness tensor and ∇u represents the gradient of the displacement field within the operative design space.

The Lagrangian density, as the integrand of the functional in Equation (S1), is formulated as follows:

$$\mathcal{L} = \frac{1}{2} k_a \left(\frac{\partial u}{\partial a} \right)^2 + \frac{1}{2} k_g \left(\frac{\partial u}{\partial g} \right)^2 - \tilde{f} \cdot u \tag{S2}$$

Postulating that the postoperative steady state corresponds to an extremum of the total energy functional, the governing condition is enforced by the Euler–Lagrange equation as follows:

$$\frac{\partial \mathcal{L}}{\partial u} - \frac{\partial}{\partial a} \left(\frac{\partial \mathcal{L}}{\partial (\partial u / \partial a)} \right) - \frac{\partial}{\partial g} \left(\frac{\partial \mathcal{L}}{\partial (\partial u / \partial g)} \right) = 0 \tag{S3}$$

Substituting Equation (S2) into Equation (S3) and carrying out functional differentiation yields the following explicit field equation:

$$-\tilde{f} - \frac{\partial}{\partial a} \left(k_a \frac{\partial u}{\partial a} \right) - \frac{\partial}{\partial g} \left(k_g \frac{\partial u}{\partial g} \right) = 0 \tag{S4}$$

Under a local linearization assumption, Equation (S4) simplifies to the following:

$$k_a \frac{\partial^2 u}{\partial a^2} + k_g \frac{\partial^2 u}{\partial g^2} = -\tilde{f} \tag{S5}$$

The normalization of Equation (S5) yields the canonical dimensionless governing law, termed the Kinematic Conflict Equation (KCE):

$$\frac{\partial^2 u}{\partial a^2} + k \frac{\partial^2 u}{\partial g^2} = f \tag{S6}$$

where $k = k_g / k_a$ and $f = -\tilde{f} / k_a$.

Solving the homogeneous KCE (with the forcing term set to zero) by separation of variables, $u(a, g) = A(a)G(g)$, yields the following analytical solution:

$$u(a, g) = (C_1 e^{\sqrt{|\lambda|}a} + C_2 e^{-\sqrt{|\lambda|}a})(D_1 \cos(\omega g) + D_2 \sin(\omega g)) \tag{S7}$$

where the separation constant λ is taken to be negative for the oscillatory solution branch and ω sets the spatial oscillation scale of the separated solution.

From the harmonic component of Equation (S9), the characteristic tolerance period (T) of the implant geometry is derived as follows:

$$T = \frac{2\pi}{\omega} = 2\pi \sqrt{\frac{k}{|\lambda|}}, \omega = \sqrt{|\lambda| / k} \tag{S8}$$

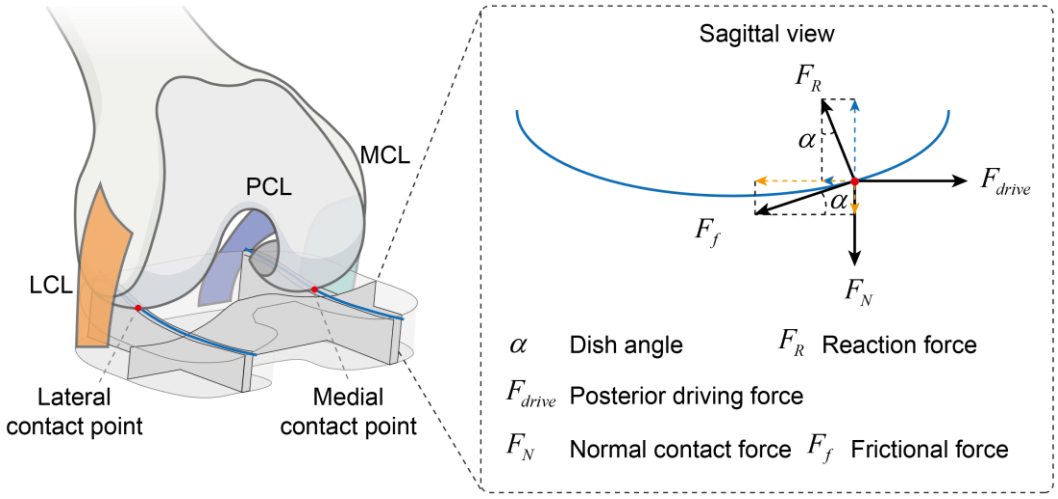
where k governs the aperture of the admissible kinematic basin and defines the system's stability phases as follows:

- Underconstrained: Large T → hypersensitive system with unstable kinematics;

- Solvable: A stable basin exists, requiring coordinated $a-g$ adjustment to minimize residuals; and
- Overconstrained: The tolerance zone collapses; no feasible $a-g$ combination restores compatibility.

A2. Derivation of the kinematic pattern equation

At the tibiofemoral interface, the reconstructed system is formulated as a constrained equilibrium of four principal force vectors representing the compartmental compressive force F_N, the posterior driving force F_{drive}, the reaction force F_R, and the frictional force F_f.



Supplementary Fig. 1 | Force-balance model at the tibiofemoral contact interface used to derive the kinematic pattern equation.

Left, schematic representation of the reconstructed tibiofemoral joint showing the medial and lateral contact points and the principal soft-tissue constraints, including the medial collateral ligament (MCL), lateral collateral ligament (LCL) and posterior cruciate ligament (PCL). Right,

local sagittal-plane force decomposition at a representative tibiofemoral contact point. F_N denotes the normal compressive force, F_R the articular reaction force, F_f the tangential frictional force and F_{drive} the posterior driving force. The local articular-surface inclination is represented by the dish angle α. Resolution of these forces in the horizontal and vertical directions provides the equilibrium relations used in the derivation of the kinematic pattern equation (KPE).

The force-balance equations were obtained by requiring the net forces in the vertical and horizontal directions to vanish:

$$\begin{cases} F_R \cos\alpha - F_f \sin\alpha = F_N \\ F_R \sin\alpha + F_f \cos\alpha = F_{drive} \end{cases} \tag{S9}$$

where α denotes the tibial plateau dish angle, defined here as the local inclination of the concave tibial articular surface at the contact point relative to the nominal tibial plateau plane. This angle determines how the resultant contact force is resolved into the compressive normal force and the posterior driving component.

Combining the two component-balance equations in Equation (S9) yields the relation between the posterior driving force and compressive force as follows:

$$F_{drive} = F_N \cdot \left(\frac{\sin\alpha + \mu\cos\alpha}{\cos\alpha - \mu\sin\alpha} \right) \tag{S10}$$

By defining the friction angle as $\mu = \tan\phi$, Equation (S10) simplifies to the following:

$$F_{drive} = F_{resist} = F_N \tan(\alpha + \phi) \tag{S11}$$

By introducing the posterior tibial slope α_s, the effective geometric resistance is modified, and

Equation (S11) is expressed under the stated frictionless approximation as follows:

$$F_{resist} \approx F_N \tan(\alpha - \alpha_s) = kx\left(\tan^2 \alpha - \tan\alpha \tan\alpha_s\right) \tag{S12}$$

Enforcing the equilibrium condition by substituting the compartmental stiffness coefficients and rollback displacements into the force-balance law yields the following expression:

$$k_{post} \frac{x_{med} + x_{lat}}{2} \cos^2 \theta_p = k_{med} x_{med} (\tan^2 \alpha_{med} - \tan\alpha_{med} \tan\alpha_s) + k_{lat} x_{lat} (\tan^2 \alpha_{lat} - \tan\alpha_{lat} \tan\alpha_s) \tag{S13}$$

We then define

$$S = \frac{K_{med}}{K_{lat}}, \quad Q = \frac{K_{post}}{K_{med}}, \quad R = \frac{x_{lat}}{x_{med}} \tag{S14}$$

where S represents the medial-to-lateral relationship in effective soft-tissue constraints, Q represents posterior drive relative to medial anchoring, and R represents the differential rollback ratio. Collecting the geometry-dependent terms into the effective coefficients γ_1, γ_2, and γ_3, Equation (S13) reduces to the kinematic pattern equation

$$R = \frac{S(\gamma_1 Q - \gamma_2)}{\gamma_3 - \gamma_1 SQ} = \frac{Q - Q_L}{Q_U - Q}, \quad Q_L = \frac{\gamma_2}{\gamma_1}, \quad Q_U = \frac{\gamma_3}{S\gamma_1} \tag{S15}$$

Equation (S15) has a hyperbolic form. For the physically admissible branch considered here, positive posterior rollback occurs within the interval:

$$Q_L < Q < Q_U(S) \tag{S16}$$

and R increases monotonically with Q. A necessary condition for this admissible interval to exist is therefore

$$Q_L < Q_U(S) \tag{S17}$$

or

$$\frac{\gamma_2}{\gamma_1} < \frac{\gamma_3}{S\gamma_1} \tag{S18}$$

$$S < S_{crit} = \frac{\gamma_3}{\gamma_2} \tag{S19}$$

Thus, the KPE itself predicts an upper admissible boundary for S. As S approaches S_{crit} from below, the upper and lower Q boundaries converge and the admissible Q interval collapses:

$$\Delta Q(S) = Q_U - Q_L = \frac{1}{\gamma_1}\left(\frac{\gamma_3}{S} - \gamma_2\right) \to 0 \quad as \;\; S \to S_{crit} \tag{S20}$$

Within the admissible domain $0 < S < S_{crit}$, the sensitivity of rollback to the flexion-state metric is

$$\frac{\partial R}{\partial Q} = \frac{S\gamma_1\left(\gamma_3 - \gamma_2 S\right)}{\left(\gamma_3 - \gamma_1 SQ\right)^2} > 0 \tag{S21}$$

Therefore, the KPE yields two related predictions. First, S is not an unrestricted parameter but is bounded above by a critical value determined by the effective geometric coefficients. Second, the admissible range of Q is conditional on S: increasing S progressively narrows the available Q interval until it collapses at $S = S_{crit}$. Within this admissible domain, Q provides a monotonic coordinate for transition among rollback states.

A3. Jacobian mapping and energy–force equivalence between the KCE and KPE

To bridge the surgical design space and the physical state space, we formulated the Jacobian sensitivity matrix, $\mathbf{J}$, as follows:

$$\mathbf{J} = \frac{\partial \boldsymbol{y}}{\partial \mathbf{p}} = \begin{bmatrix} \frac{\partial x_{vmed}}{\partial a} & \frac{\partial x_{vmed}}{\partial g} \\ \frac{\partial x_{vlat}}{\partial a} & \frac{\partial x_{vlat}}{\partial g} \end{bmatrix} \tag{S22}$$

where $\mathbf{p} = [a, g]^T$ denotes the generalized surgical vector and $\boldsymbol{y} = [x_{vmed}, x_{vlat}]^T$ represents the physical displacement vector.

Under a small perturbation of the surgical state, the corresponding physical displacement perturbation satisfies the following equation:

$$\delta \boldsymbol{y} = \mathbf{J} \delta \mathbf{p} \tag{S23}$$

In the physical space, the local elastic energy stored in the soft-tissue envelope can be written as follows:

$$V_{phy} = \frac{1}{2} \delta \boldsymbol{y}^T k_{phy} \delta \boldsymbol{y}, \quad k_{phy} = diag(k_{med}, k_{lat}) \tag{S24}$$

Substituting Equation (S23) into the above equation yields the equivalent energy expression in the surgical design space as follows:

$$V_{phy} = \frac{1}{2} \delta \boldsymbol{p}^T \boldsymbol{J}^T k_{phy} \boldsymbol{J} \delta \boldsymbol{P} \tag{S25}$$

The proposed stiffness representation in the surgical design space is written as follows:

$$k_{param} = diag(k_a, k_g) = \boldsymbol{J}^T k_{phy} \boldsymbol{J} \tag{S26}$$

On the basis of the principle of virtual work, the forces in the physical space can be mapped to the surgical design space as follows:

$$\begin{bmatrix} \frac{\partial x_{vmed}}{\partial a} & \frac{\partial x_{vlat}}{\partial a} \\ \frac{\partial x_{vmed}}{\partial g} & \frac{\partial x_{vlat}}{\partial g} \end{bmatrix} \begin{bmatrix} k_{med} x_{vmed} \\ k_{lat} x_{vlat} \end{bmatrix} = \begin{bmatrix} f_a \\ f_g \end{bmatrix} \tag{S27}$$

Considering the force balance in the direction of the geometric constraint, we obtain the following expression:

$$\frac{\partial x_{vmed}}{\partial g}\left(k_{med} x_{vmed}\right) + \frac{\partial x_{vlat}}{\partial g}\left(k_{lat} x_{vlat}\right) = f_g \tag{S28}$$

The geometric parameter, g, modulates the implant slope, yielding the following relationship between the displacement gradient and the slope angle:

$$\frac{\partial x_{vmed}}{\partial g} = \tan \alpha_{med}, \frac{\partial x_{vlat}}{\partial g} = \tan \alpha_{lat} \tag{S29}$$

The geometry-dependent driving-force formulation used in the model is written as follows:

$$F_{drive} = k_{med} \tan^2 \alpha_{med} \cdot x_{med} + k_{lat} \tan^2 \alpha_{lat} \cdot x_{lat} \tag{S30}$$

Since the surgical posterior tibial slope (α_s) skews the effective horizontal reference plane, this geometric identity requires a coordinate transformation before physical rollback can be mapped back to the operative design space as follows:

$$F_{drive} = k_{med} x_{med} \tan^2(\alpha_{med} - \alpha_s) + k_{lat} x_{lat} \tan^2(\alpha_{lat} - \alpha_s) \tag{S31}$$

Equation (S31) is compared with the KPE derived independently from Newtonian force-balance conditions.

A4. In situ decoupling of the soft-tissue constraint tensor

We used an *in situ* decoupling algorithm to convert the coupled gap responses measured by the TKA Balance Solver into effective components of the soft-tissue constraint tensor. The solver captures the integrated compartment-level soft-tissue response. We therefore treated the solver output as a coupled mechanical response field and decomposed it into angle-specific effective stiffness components.

Under the equivalent beam–spring model (Fig. 3e), controlled joint-distraction loading applies medial and lateral separating forces to open the tibiofemoral gap and tension the collateral restraints. The response was represented by the following force- and moment-balance equations:

$$\begin{cases} F_{med} + F_{lat} = K_{med}\Delta H_{med} + K_{lat}\Delta H_{lat} \\ \dfrac{L}{m}F_{med} - \dfrac{L}{m}F_{lat} = \dfrac{L}{2}K_{med}\Delta H_{med} - \dfrac{L}{2}K_{lat}\Delta H_{lat} \end{cases} \tag{S32}$$

where F denotes the distractive force applied via the solver, ΔH represents the change in the compartmental gap, K_{med} and K_{lat} denote the effective stiffnesses of the medial and lateral compartments, respectively.

At each flexion angle, the compartmental force–gap responses were fitted by multiple linear regression using the following model:

$$H = H_0 + aF_{med} + bF_{lat} \tag{S33}$$

The intercept, H_0, was interpreted as the extrapolated gap at zero applied distraction force ($F = 0$) and served as the reference for estimating gap deformation from the measured loading responses.

Under the equivalent mechanical model, the resulting force–gap relationships yield the following

effective stiffness estimators:

$$\begin{cases} K_{med} = \dfrac{(m+2)F_{med} + (m-2)F_{lat}}{2m\Delta H_{med}} \\ K_{lat} = \dfrac{(m+2)F_{lat} + (m-2)F_{med}}{2m\Delta H_{lat}} \end{cases} \tag{S34}$$

Taking the ratio of these two expressions gives the medial-to-lateral constraint ratio:

$$S(\theta) = K_{med}(\theta) / K_{lat}(\theta) \tag{S35}$$

In the first-order equivalent-stiffness model, the contributions of the posterior capsule and posterior cruciate ligament (PCL) in near extension were assumed to be small relative to the collateral restraints. The measured compartmental stiffnesses were therefore approximated by the corresponding baseline collateral stiffnesses:

$$K_{med}(10^\circ) \approx K_{MCL}(10^\circ), \quad K_{lat}(10^\circ) \approx K_{LCL}(10^\circ) \tag{S36}$$

At 90° of flexion, by introducing collateral relaxation coefficients ($\rho(\theta)$) and assuming a consistent force–excursion reference between early and deep flexion, the governing relationship is formulated as follows:

$$K_{post}(90^\circ) = K_{med}(90^\circ) + K_{lat}(90^\circ) - \rho_{med} K_{med}(10^\circ) - \rho_{lat} K_{lat}(10^\circ) \tag{S37}$$

The deep-flexion relaxation coefficients, ρ_{med} and ρ_{lat}, were set to 0.80 and 0.50, respectively, for the primary analysis, representing retention of 80% of the medial and 50% of the lateral early-flexion collateral contributions at 90° of flexion. These coefficients were calibrated using intraoperative compartmental measurements obtained from a patient who underwent PCL resection and were subsequently applied uniformly across the primary cohort. Once the scaled

medial and lateral collateral contributions are specified, the effective posterior constraint, $K_{post}\left(90^{\circ}\right)$, can then be estimated as the residual contribution under the stated model assumptions. The flexion-state metric Q is then defined by normalizing this posterior constraint to the medial anchoring stiffness at the same flexion angle:

$$Q(\theta) = \frac{K_{post}(\theta)}{K_{med}(\theta)} \tag{S38}$$

At 90° of flexion, *Q* was evaluated from Equation (S38) using the estimated effective posterior and medial stiffnesses. This dimensionless coordinate describes posterior constraint relative to medial anchoring. By contrast, *S* characterizes the medial-to-lateral effective constraint relationship. Together, *S* and *Q* capture complementary aspects of the patient-specific soft-tissue state derived from the same intraoperative force–gap measurements.

Collectively, in situ decoupling converts measured compartment-specific force–gap responses into effective medial, lateral and posterior stiffness estimates, from which the measurable coordinates *S* and *Q* are obtained. These coordinates link the intraoperative solver measurements to the KPE: *S* characterizes extension-state constraint structure, whereas *Q* characterizes the flexion-state posterior-to-medial constraint relationship. Their associations with the observed differential rollback ratio *R* are examined in the subsequent analyses.

A5. Processing and integration of intraoperative kinematic trajectories

For each valid intraoperative kinematic recording, medial and lateral tibiofemoral contact-point trajectories were reconstructed from the tracked relative joint motion. Compartment-specific anteroposterior displacements were calculated over the prespecified 30°–90° flexion interval. The path-level differential rollback ratio was defined as follows:

$$R(\theta) = \frac{x_{lat}}{x_{med}} \tag{S39}$$

where x_{lat} and x_{med} denote the lateral and medial posterior displacements, respectively, for path i. Path-level trajectories were classified as paradoxical anterior translation ($R < 0$), lateral-pivot rollback ($0 < R < 1$) or medial-pivot rollback ($R > 1$).

Some knees had multiple valid intraoperative trajectories acquired under different surgical states, including changes in component position or soft-tissue release. These recordings were retained as distinct path-level observations for analyses of rollback-phase boundaries. For analyses requiring a single representative kinematic trajectory per knee, repeated paths were combined using an energy-based weighting procedure. The resulting representative trajectory was a model-based summary and not an additional recorded motion cycle.

For the weighting procedure, the elastic energy associated with each trajectory was estimated from compartment-specific effective stiffness and the corresponding posterior displacement over the 30°–90° flexion interval. Effective stiffness values between measured flexion states were linearly interpolated at 10° intervals. Each trajectory was assigned the following normalized exponential energy weight:

$$\omega_i = \frac{\exp\left(-E_i / \bar{E}\right)}{\sum_{j=1}^{n} \exp\left(-E_j / \bar{E}\right)}, \quad \bar{E} = \frac{1}{n}\sum_{i=1}^{n} E_i \tag{S40}$$

where E_i is the total energy associated with path i, $\bar{E}$ is the arithmetic mean of the energies of the n valid paths from the same knee, and ω_i is the normalized path weight. Lower-energy trajectories therefore received greater weights. The representative knee-level trajectory was calculated as

$$\bar{P} = \sum_{i=1}^{n} \omega_i P_i \tag{S41}$$

where P_i denotes the i th path-level trajectory. The knee-level differential rollback ratio was subsequently calculated from the medial and lateral displacements of the integrated trajectory using the same definition as for path-level R.

Within-knee path consistency was evaluated separately from the energy-weighted integration. For each recorded path, a phase angle was defined as follows:

$$\Phi_i = \arctan\left(R_i\right) \tag{S42}$$

Within-knee phase-angle dispersion was then quantified as follows:

$$\Delta\Phi = \max_i\left(\Phi_i\right) - \min_j\left(\Phi_j\right) \tag{S43}$$

Knees in which all available path-level R values remained within the same rollback phase region were classified as the stable-basin subset. The high-confidence stable subset additionally required a within-knee phase-angle range of $\Delta\Phi \le 0.15$ radians. These subset definitions were used only for sensitivity analyses of rollback-phase stability and did not alter the primary path-level threshold analyses.